Numerical and analytical introduction to the prediction of grain boundary micro-crack initiation induced by slips bands impingement. Effect of material and microstructure parameters.

Mohamed Ould Moussa[1,*], **Maxime Sauzay**[1]

[1] CEA, DEN, DANS, DMN, SRMA, F-91191Gif-sur-Yvette, France

* Corresponding author: mohamed.ouldmoussa@cea.fr

Abstract

Micro-cracks are often observed at the intersections of thin slip bands (SB) and grain boundaries (GB) due to local stress concentration. Numerous models are based on the pile-up theory and the Griffith criterion, used since the pioneering work of Stroh. We have shown that the former underestimate strongly the macroscopic stress for GB micro crack nucleation. In fact, the key issue is that slip bands display finite thickness, observed to belong to [20nm 1000nm]. Therefore, one aims to account for the effect of SB thickness in crystalline finite element (FE) calculations performed using the Cast3M software. The simulations take into account the effects of isotropic elasticity parameters, cubic elasticity, GB orientation and crystallographic orientation of the considered grain. Following the theory of matching of asymptotic expansions, this leads to an analytical expression of the GB normal and shear stress, which show weaker stress singularities than the pile-up one.

Keywords Micro-cracks, slip bands, pile-up theory, linear fracture mechanics, FE method, crystalline plasticity

1. Introduction

Many issues are available dealing with the appearance and effects of either slip bands (SBs) or dislocation channels on the behavior of irradiated materials. Indeed, the intersection sites between SBs and grain boundaries (GBs) are prone to micro-crack nucleation because of strain localization. A series of papers [1 ; 2 ; 3 ; 4 ; 5 ; 6] highlight the presence of slip localization in Faced Centred Cubic (FCC) metals and alloys observed after post-irradiation tensile loading. Slip Bands were also observed in [7 ; 8 ; 9 ; 10 ; 11 ; 12 ; 13 ; 14] after cyclic loading. Such slip bands have been shown to be Persistent Slip Bands (PSBs) [9]. Some other works [15] have reported the formation of Slip Bands appearing during simple tensile loading. Whatever the loading conditions, such slip bands show a thickness lying between ten nanometers and a few micrometers, and a length about the grain size, usually varying from ten micrometers to a few hundred micrometers. Jiao *et al.* [5] have evidenced strong localization in austenitic stainless steels in post-irradiation tensile tests, using AFM measurements. Wejdemann and Pedersen [16] have applied the same techniques to observe such localization in the PSBs where plastic strain is shown to be fifty times larger than the macroscopic plastic strain. Sharp [1] and Edwards et al. [4] highlighted strain localization in single crystal and polycrystals of copper subjected to post-irradiation tensile loadings. Sauzay *et al.* [17] confirmed such localization in the case of irradiated austenitic stainless steels.

In addition, several works attempted to model the stress concentration at grain boundaries. Besides, it is proved that the anisotropy character of crystalline elasticity induces stress concentration at grain boundaries according to Neumann [18]. Margolin and co-workers [19 ; 20] have carried out optical observations of slip traces and conclude that stresses are more concentrated near grain boundaries. The stress gradients around GBs, induced by plastic deformation incompatibilities between neighbor grains, can be tracked thanks to large-scale finite element (FE) computations [21].

Such stress concentrations may allow to induce inter-granular crack initiation because they neglect plastic slip localization. Therefore, in the scope of the current contribution, one investigates the effect of localized slip on GB stress fields.

An analytical approach, based on the well-known Stroh model [22], has been largely applied in order to evaluate GB stress. One recurrent issue has indeed been, since decades, the using of discrete or continuous dislocation pile-ups. The stress singularity, due to an edge or screw pile-up of length $L^{Pile\text{-}up}$ has been shown to be the same as the one of a crack in the framework of linear elastic fracture mechanics (LEFM) [22 ; 23]. Therefore, an energy criterion has been proposed by [23], based on the Griffith criterion, for predicting micro-crack nucleation. The latter may be used for the case of a singularity exponent of 0.5 only and it fails when the exponent value is less than 0.5 because the energy release rate, G, becomes equal to zero [24 ; 25]. Cottrell [26] later suggested that the fracture process should be controlled by the critical crack growth stage under the applied tensile stress, which required higher stress than the crack nucleation itself as suggested by Stroh. Cottrell came with a modeling by supposing that slip occurs along two atomic planes which intersection shows pile-up dislocation.

However, Sauzay and Evrard [17] recently have outcame with the limitation of such basic pile-up theory to more accurately predict micro-crack initiation. Following their work, the pile-up theory leads to an underestimation of macroscopic stresses with comparison to experimental data. Indeed, the pile-up approach postulates that slip localization occurs on one atomic plane only, but, experiments carried out using various materials and loading conditions show slip occurring on many slip atomic planes [8], [27], [5 ; 16], [28]. Therefore, because of the distribution of plastic slip through the slip band thickness [2 nm, 1000 nm], accounting for the SB thickness in the models may improve the predictions.

The current contribution aims to validate an analytical model of GB stress fields in the case of SB impingement. Then, the first section presents the analytical modeling for close stress fields configuration which corresponds to points located near the intersection of the GB and the SB. The second section deals with finite element (FE) calculations in order to investigate numerically the effect of SB or GB geometry and material properties on GB stress fields. Besides, a final section is devoted, on one side, to adjust parameters and validate the analytical model and on the other side, to show the influence of GB and SB orientation on the adjusted model parameters and a conclusion will end the paper.

2. Analytical modeling

The subsequent problem is to be solved: an elastoplastic slip band is embedded at the free surface of an elastic matrix, subjected to a displacement controlled tensile loading (Fig. 1a).

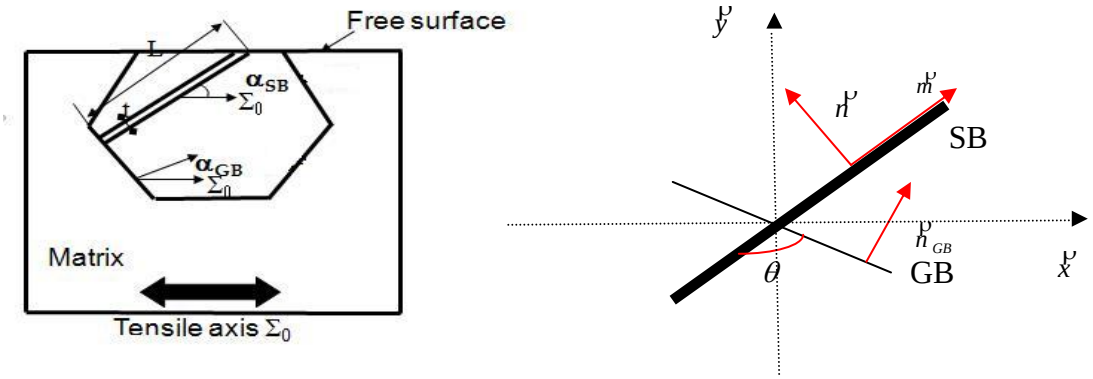

a) b)

Figure 1. a) Main grain, slip band and matrix b) SB-GB intersection and associated vectors

Fig. 1a and b show the following parameters:

- SB and GB orientation related ones:

  $\vec{m}\,(=\frac{1}{\sqrt{2}}(1,0,-1))$, $\vec{n}\,(=\frac{1}{\sqrt{3}}(1,1,1))$, $\vec{n}_{GB}, \alpha_{SB}, \alpha_{GB}$ and θ denote respectively slip direction vector, normal vector to slip plane, normal vector to the GB, angle between slip plane and loading direction $(\vec{m}, \vec{x})$, angle between the GB normal and loading direction $(\vec{n}_{GB}, \vec{x})$ and an angle between the SB and the GB, given by:

  $$\theta = 90^o - \alpha_{SB} + \alpha_{GB}. \qquad (1)$$

- SB size and loading parameters: t, L, Σ_0 and f are respectively SB thickness, SB length, macroscopic applied tensile stress and Schmid factor.

In addition, for further assumptions, let $\sigma_{nn}, \sigma_{nm}, \tau_0$ and r be respectively the GB normal stress, the GB shear stress, SB yield shear stress and the distance to the SB along the GB. It is worth to note that the developments involved in the current paper concern the close fields configuration which means that one focuses on stress evolution near the intersection of the SB and the GB (at a distance r such as 0 < r << t). The point located at the intersection of SB and GB corresponds to r = 0.

GB stresses singularity is the same as the crack one in the LEFM framework, leading to an exponent of 0.5 of the stress expansion. [22 ; 23], the GB normal stress field induced by one edge dislocation pile-up is given by:

$$\sigma_n^{pile\text{-}up}(r,\theta) = \frac{3}{2}\left(L^{pile\text{-}up}/r\right)^{1/2}(f\Sigma_0 - \tau_0)h(\theta) + \Sigma_n^{\infty}, \qquad (2)$$

where $h(\theta) = \sin\theta\cos(\theta/2), \Sigma_n^{\infty} = \Sigma_0\cos^2(\alpha_{GB})$ and $L^{pile-up} = L/2$.

The absence of any term accounting for the SB thickness, t, in Eq. 2 is noticeable. Indeed, slip is assumed to occur on one atomic plane only as mentioned earlier.

However, experimental observations have shown that slip may occur in many atomic plane and lead to the question of taking into account SB thickness. This implies the existence of two characteristic lengths: SB length and thickness, in the new problem of finite thickness. It is also proved [17] that the driving force $(f\Sigma_0 - \tau_0)$ is proportional to the macroscopic shear stress. These two points make our problem be similar to the case of a crack with a V-noch tip in an elastic matrix even the stress singularity is induced by a slip localization in ours. That is why, following the theory of matching expansions [24 ; 29], we perform a modeling of the GB normal and shear stress close fields with respect to the SB length, L and the SB thickness, t:

$$\sigma_{nn}(r) = A_{nn}\left(L/t\right)^{0.5}\left(t/r\right)^{\alpha}(f\Sigma_0 - \tau_0), \qquad (3)$$

and

$$\sigma_{nm}(r) = A_{nm}\left(L/t\right)^{0.5}\left(t/r\right)^{\alpha}(f\Sigma_0 - \tau_0). \qquad (4)$$

α is the singularity exponent A_{nn} and A_{nm} are model parameters. The subscript “nn” corresponds to the GB normal stress and “nm” to the GB shear stress.

It is worth to highlight that this model assumes a linear dependence of GB stresses on the driving shear stress, $T = f\Sigma_0 - \tau_0$, and the same singularity exponent is valid for both shear and normal stress components and whatever L and t. The main difference between this model and the pile-up one is that the finite SB thickness, t, is taken into account. The stress singularity is assumed to be weaker in the proposed model than in the pile-up case, $\alpha < 0.5$ as it will be probably shown.

3. Finite Elements (FE) calculations

3.1. FE model and loading

A 2D matrix is considered, embedding a surface grain, main grain (MG), which contains a slip band. Constitutive laws in each material are:

- Both isotropic and cubic elasticity laws in SB. As shown in Fig. 2a, it is characterized by a quasi-perfect-plastic flow, indeed, a low hardening coefficient ($H_0 \sim$ 1MPa) is assumed for avoiding numerical convergence problems. Only, one slip system is activated in the SB, which slip plane is (111) and slip direction is $[10\bar{1}]$. A yield stress τ_0, equals to 60 MPa, is initial SB critical shear stress.
- Both isotropic and cubic elasticity laws in the MG.
- The matrix obeys isotropic elasticity, defined by a Young's modulus and Poisson ration values.

Crystalline FE elements are used in the mesh shown in Fig. 2b to allow FE calculations using Cast3M code. A tensile loading is imposed along $\underline{x}$ direction and plane strain is assumed. In addition, many FE computations proved that this model is insensitive to both the mesh size and the time stepping.

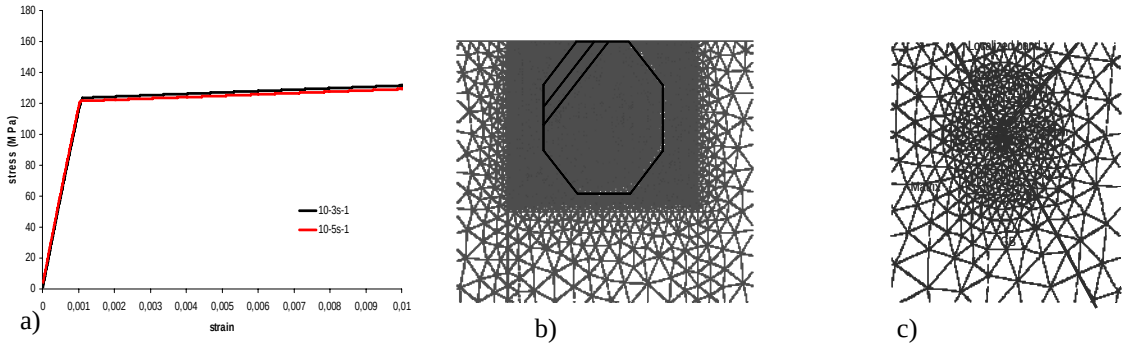

Figure 2.a) Perfect plasticity behavior of the slip band b) Zoom on the mesh: main grain (MG) and slip band (SB) c) Intersection of the SB and the GB.

The applied tensile stress Σ_0 is high enough to lead to slip band plastic flow and (Table 1) shows both isotropic and cubic elasticity parameters used in the calculations [30]. C_{11}, C_{12} and C_{44} are the crystalline elasticity parameters.

Table 1. Isotropic and cubic elasticity parameters

E (in matrix, MG and SB)		180 GPa
ν (in matrix, MG and SB)		0.33
	Isotropic elasticity (MG and SB)	Cubic elasticity (MG and SB)
C_{11}	267 GPa	267 GPa
C_{12}	131 GPa	131 GPa
C_{44}	68 GPa	224.4 GPa
a	1	3.3

The anisotropy coefficient is defined by $a = 2C_{44} / C_{11} - C_{12}$ and if it equals to one, crystalline elasticity is isotropic. In case of copper or austenitic stainless steel, the Young's modulus along the <111> directions is more than 3 times the one along the <100> directions. That is why it would be worth to numerically account for such anisotropy in our contribution.

3.2. Effect of the variation of GB and SB geometry

This part shows the effect of SB characteristic lengths on the GB normal and shear stresses. The length effect may be studied using Fig. 3 a) and b) and the thickness one using Fig. 4 a) and b). One assumes that crystalline elasticity is isotropic ($a = 1$).

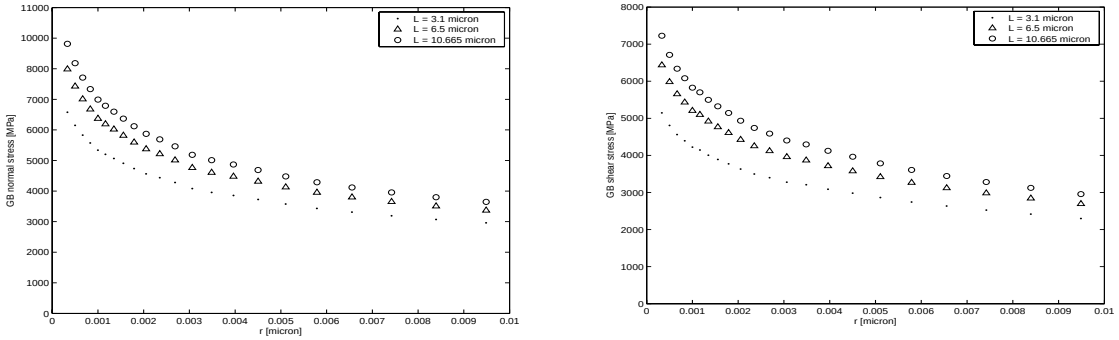

a) b)

Figure 3. a) GB normal stress b) GB shear stress, with respect to the distance to the GB-SB intersection in close field configuration for: austenitic stainless steel, t=0.09 μm, Σ_0 = 878 MPa, α_{GB} = 33°, α_{SB} = 45°, τ_0 = 60 MPa

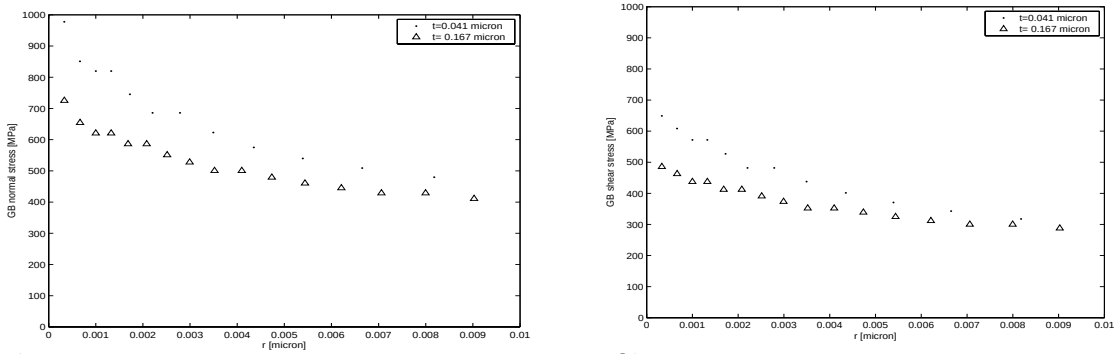

a) b)

Figure 4. a) GB normal stress b) GB shear stress, with respect to the distance to the GB-SB intersection in close field configuration for: austenitic stainless steel, L=10.71 μm, Σ_0 = 174 MPa, α_{GB} = 33°, α_{SB} = 45°, τ_0 = 60 MPa

Besides, one can observe: the higher the SB length the higher the GB normal and shear stresses, as also expected from the pile-up theory. However, the higher the SB thickness the lower the GB stresses. Physically, that highlights that very narrow SBs should lead to easier GB micro-crack nucleation than large ones.

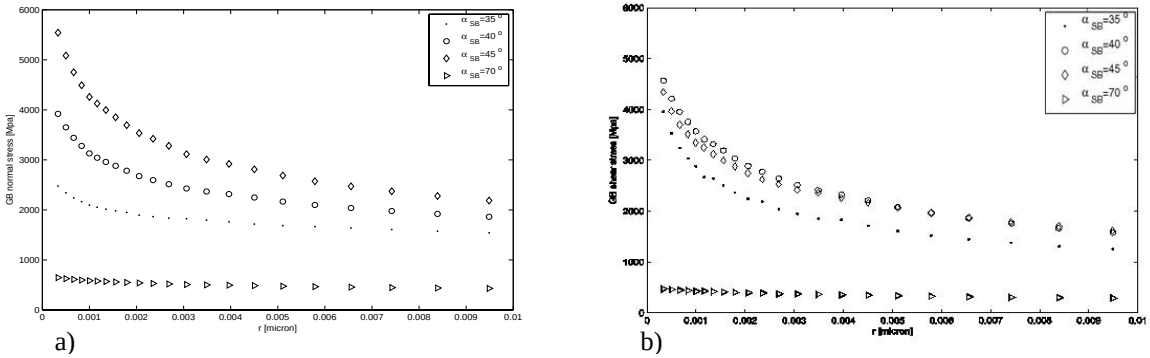

a) b)

Figure 5. a) GB normal stress b) GB shear stress, with respect to the distance to the GB-SB intersection in close field configuration for: Austenitic stainless steel, L=10.71 μm, t=0.09 μm, Σ_0 = 393 MPa, α_{GB} = 33°, τ_0 = 60 MPa

Moreover, GB and SB orientations are proved to induce strong change in GB stress fields. That is

why the normal and shear stress fields are computed for different values of α_{SB} and α_{GB}. The GB normal stress reaches a maximum peak for α_{SB} equal to 45° because of the corresponding highest Schmid factor value (f = 0.5). For lower or higher α_{SB} values, the normal stress is lower (Fig. 5 a)) and the same almost occurs to the shear stress (Fig. 5 b)). Indeed, a lower Schmid factor leads to delayed plastic flow and low plastic slip which induces the stress concentration.

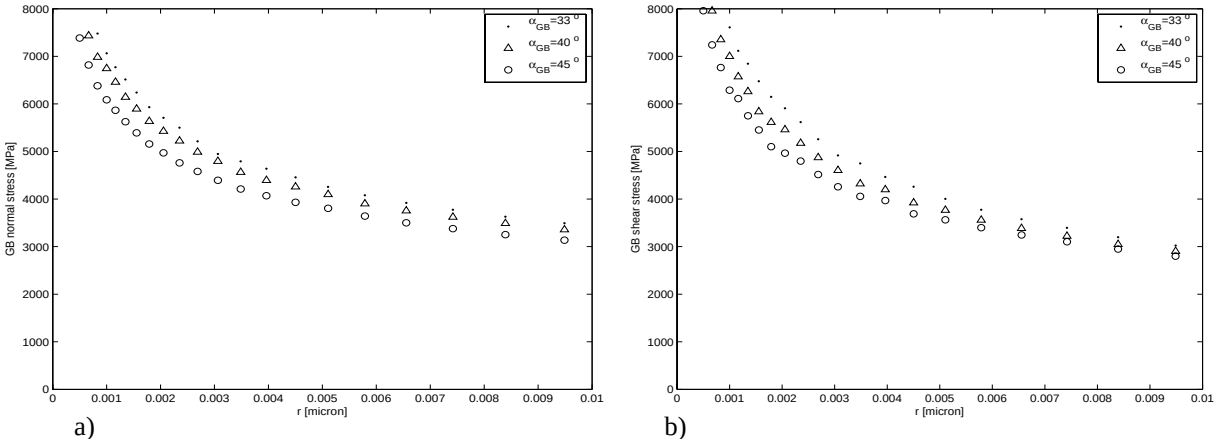

a) b)

Figure 6. a) GB normal stress b) GB shear stress, with respect to the distance to the GB-SB intersection in close field configuration for: Austenitic stainless steel, L=10.71 μm, t=0.09 μm, Σ_0 = 878 MPa, α_{SB} = 45°, τ_0 = 60 MPa

Concerning the GB orientation, the results show that GB stress fields slightly decrease with respect to α_{GB} (see Fig. 6 a) and b)).

3.3. Influence of elasticity parameters

One now aims to evaluate the influence of isotropic elasticity parameters. Fig. 7 a) and b) show GB stress fields computed for different materials, E_1 =68GPa (Aluminum), E_2 =110 GPa (Copper), E_3 = 180 GPa (Austenitic stainless steel), and corresponding Poisson ratios, ν_1 = 0.33 (Aluminum), ν_2 =

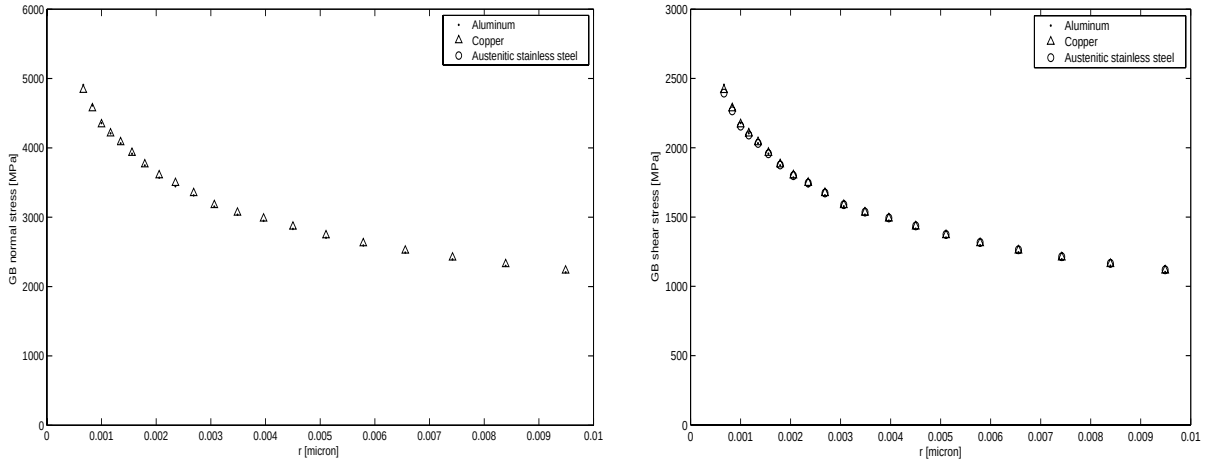

a) b)

Figure 7. a) GB normal stress b) GB shear stress, with respect to the distance to the GB-SB intersection in close field configuration for: L=10.71 μm, t=0.09 μm, Σ_0 = 393 MPa, α_{GB} = 33°, α_{SB} = 45°, τ_0 = 60 MPa

No difference with respect to these parameters is evidenced in the graphs. It has been checked that GB stresses are the same whatever the isotropic elastic parameters provided the remote tensile stress

is the same.
In copper and austenitic stainless steel, the anisotropy coefficient (Table 1) of cubic elasticity is high ($a = 3.3$), therefore, one should study the effect of such strongly anisotropic cubic elasticity on GB stress fields.

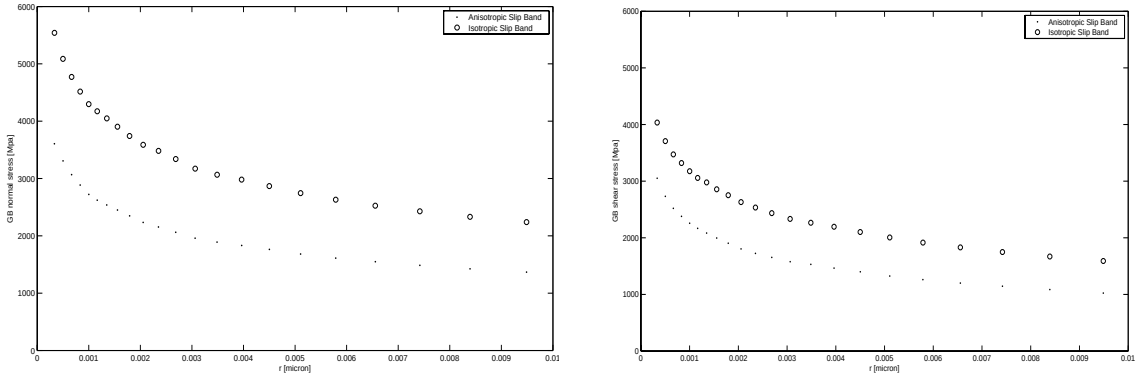

a) b)

Figure 8. a) GB normal stress b) GB shear stress, with respect to the distance to the GB-SB intersection in close field configuration for: The main grain and the SB obey either cubic elasticity or isotropic elasticity for: Austenitic stainless steel, L=10.71 μm, t=0.09 μm, $\Sigma_0 = 393$ MPa, $\alpha_{GB} = 33°$, $\alpha_{SB} = 45°$, $\tau_0 = 60$ MPa

Fig. 8 a) and b) show that cubic elasticity may affect strongly GB stresses. The latter decrease and the micro-crack nucleation cannot occur so easily than for isotropic elasticity. Indeed, in the case of anisotropic cubic elasticity, local elasticity modulus become high and Schmid factor drops (about 0.43 in this case) [30] leading to lower values of GB stress fields.

3.4. Comparison to the pile-up based model

Fig. 9 gives a comparison between our model of GB normal stress for t=0.09 mm and the pile-up GB normal stress given by Eq. 2.

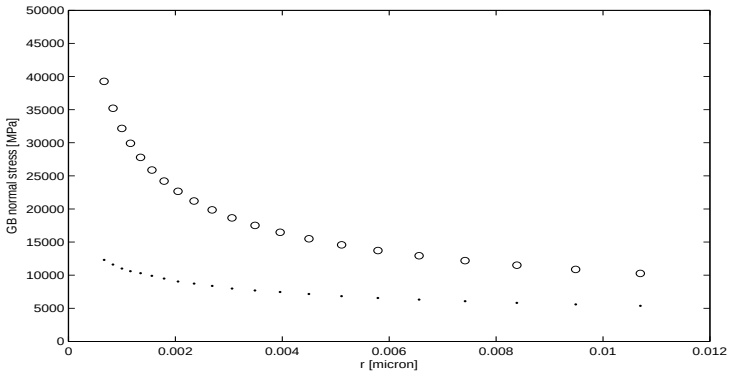

Figure 9. GB normal stress with respect to the distance to the GB-SB intersection in close field configuration for: Model (points) and Pile-up (circles) with L=10.665 μm, t=0.09 μm, $\Sigma_0 = 878$ MPa, $\alpha_{GB} = 33°$, $\alpha_{SB} = 45°$, $\tau_0 = 60$ MPa

One can clearly observe that the pile-up theory based model overestimates the GB normal stress with comparison to ours which takes into account a finite SB thickness, t. Indeed, GB normal stress seems to be about three times higher in pile-up modeling than in our approach at the same distance from the intersection of the GB and the SB.

4. Model versus FE calculations

4.1 Parameters adjustment

It is worth to note that following the theory of matching expansions [Leguillon, 2002], a same singularity exponent, α, is valid for both GB normal and shear stresses. Therefore, the current section deals with the adjustment of analytical parameters A_{nn} , A_{nm} and α in order to fit FE curves.

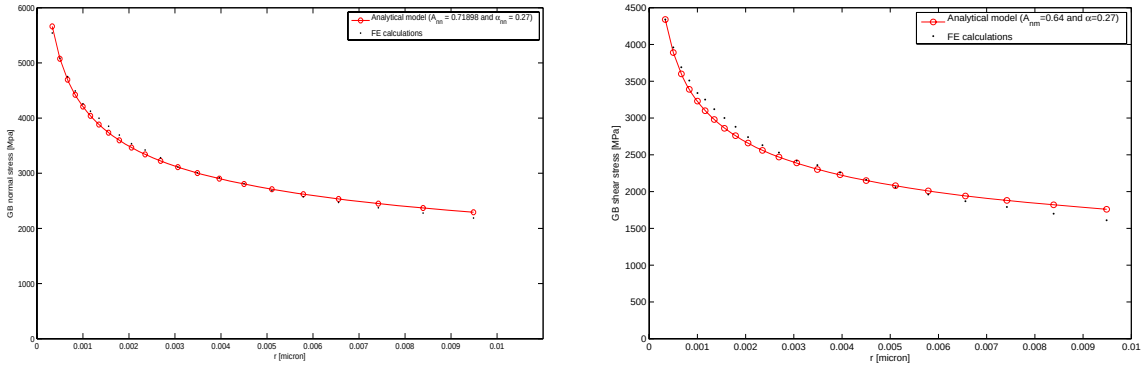

a) b)

Figure 10. a) GB normal stress (A_{nn} = 0.72) b) GB shear stress (A_{nm} = 0.64), with respect to the distance to the GB-SB intersection in close field configuration for: analytical model, Eq. 3 and 4, (red) with α = 0.27 and FE calculations (black) with L=10.71 μm, t=0.09 μm, Σ_0 = 393 MPa, α_{GB} = 33°, α_{SB} = 45°, τ_0 = 60 MPa

Fig. 10 a) and b) show a fair agreement between our optimized analytical model and the FE calculations: one suitable value of α (=0.27) is found for GB normal stress and GB shear one. As expected two different values of the factors are found depending on the chosen stress component. It takes 0.71 for the GB normal stress and 0.64 for the GB shear stress.

4.1 Validation

Let one now show the validity of our model with respect to the SB characteristic sizes (L and t). Indeed, the parameters adjustments are carried out for a new value of SB length (Fig. 11 a)) and a new one of SB thicknesses (Fig. 11 b)). For L=6.7 μm, for instance, the same parameters, A_{nn}=0.72 and α=0.27, are found and in the same manner, for t=0.04 mm, A_{nn}=0.72 and a=0.27. Therefore, we can conclude that our model is insensitive to the SB lengths for the GB normal stress.

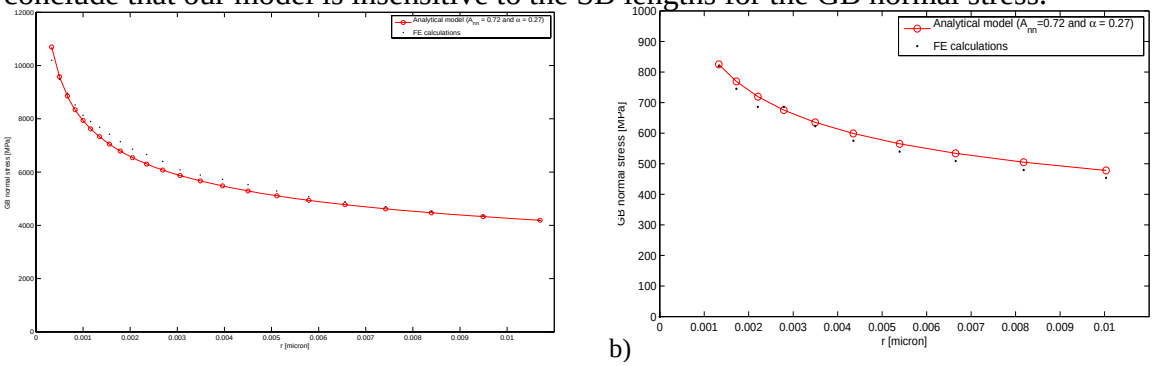

a) b)

Figure 11. a) GB normal stress (L = 6.7 μm, t = 0.09 μm, Σ_0 = 878 MPa, A_{nn}=0.72 and α = 0.27) b) GB normal stress (L = 10.665 μm, t = 0.04 μm, Σ_0 = 176 MPa, A_{nn}=0.72 and α = 0.27), with respect to the distance to the GB-SB intersection in close field configuration for: analytical model (red) and FE calculations (black) α_{GB} = 33°,α_{SB} = 45° and τ_0 = 60 MPa

4.1 Dependency on SB and GB orientation

We have performed some calculations for checking the validity of the analytical modeling with respect to GB and SB orientation (α_{GB} and α_{SB}). For the sake of simplicity, we have just carried out it for the normal corresponding parameter (A_{nn}) and it is shown in Fig. 12 a) and b) that A_{nn} and a equal respectively to 0.59 and 0.18 for $\alpha_{SB} = 35^o$ and 0.71 and 0.21 for $\alpha_{SB} = 40^o$.

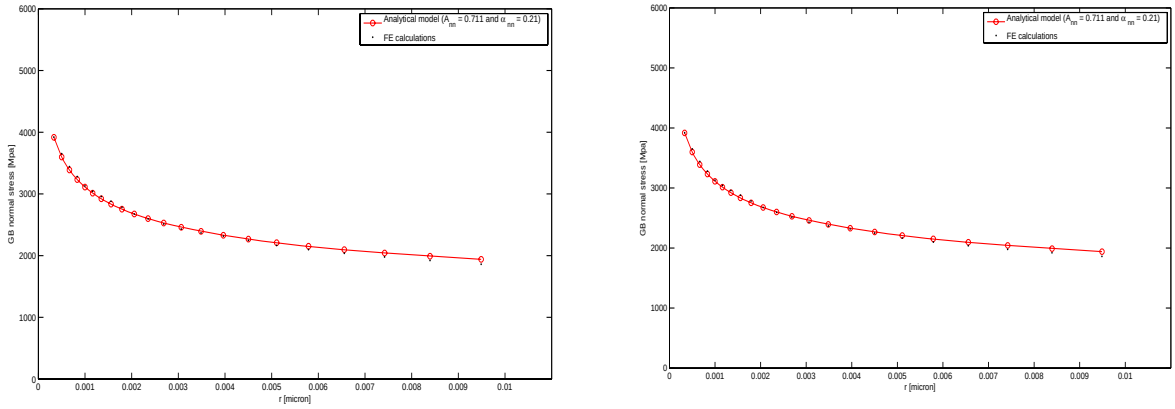

a) b)

Figure 12. a) GB normal stress (α_{SB} = 35 °, $A_{nn}(\alpha_{GB},\alpha_{SB})$=0.71 and $\alpha(\alpha_{GB},\alpha_{SB})$= 0.21) b) GB shear stress (α_{SB} = 40 °, $A_{nn}(\alpha_{GB},\alpha_{SB})$=0.59 and $\alpha(\alpha_{GB},\alpha_{SB})$= 0.18), with respect to the distance to the GB-SB intersection in close field configuration for: analytical model (red) and FE calculations (black) with L=10.665 µm, t=0.09 µm, Σ_0 = 393 MPa, α_{GB} = 33°, τ_0 = 60 MPa

Finally, we conclude that the model parameters slightly depend on the GB and SB orientation.

5. Conclusion

An analytical approach is adopted to perform a modeling of the GB stress fields with respect to the distance from the intersection of the grain boundary (GB) and the slip band (SB). It allowed tracking the stress singularity induced by the SB impingement on the GB. Afterwards, finite element calculations were computed in order to simulate the effect of the SB and GB characteristics on GB stress fields, such normal and shear components. In addition, model parameters were adjusted with respect to the involved length, thickness and angles in the problem. The model was then validated whatever the SB characteristic sizes. Finally, further works will deal with evaluating critical values (stress and crack length) in order to enhance a double criterion for the prediction of micro-crack initiation.

Acknowledgements

The current work is funded by the projects DEN/RSTB/RACOC-02-02 and DEN/RSTB/MASOL (CEA, FRANCE). Authors also acknowledge the project “FP7 Project Perform-60 Grant Agreement N° FP7-232612” for its support.

References

[1] J. V. Sharp. Phil. Mag., (1967) 16-77

[2] M. Victoria, N. Baluc, C. Bailat, Y. Dai, M. I. Luppo, R. Schäublin, B. N. Singh. J. Nucl. Mat., (2000) 276-114.

[3] E. H. Lee, M. H. Yoo, T. S. Byun, J. D. Hunn, K. Farrell, L. K. Mansur. Acta. Mater., (2001) 49-3277.

[4] D. J. Edwards, B. N. Singh, J. B. Bikde-Sorensen, Evolution of cleared channels in neutron-irradiated pure copper as a function of tensile strain. J. Nucl. Mat., 329-333(2004) 1072-1077.

[5] Z. Jiao, J. T. Busby, R. Obata, G. S. Was. Salt Lake City, Utah, 2008, pp. 379.
[6] T. S. Byun , N. Hashimoto, K. Farrell, . J. Nucl. Mat., (2006) 351-303
[7] P. Lukas, M. Knesnil, Krejci, . J. Phys. Stat. Sol., (1968) 27-545.

[8] J. M. Finney, C. Laird, Strain localization in cyclic deformation of copper single crystals. Phil. Mag., 31 (1975) 339-366.
[9] A. T. Winter, O. B. Pedersen, K. V. Rasmussen, Dislocation microstructures in fatigued copper polycrystals. Acta Metall., 29 (1981) 735-748.

[10] K. Mecke, C. Blochwitz, Saturation dislocation structures in cyclically deformed nickel single crystals of different orientations. Crystal Res. & Technol, 17 (1982) 743-758.
[11] L. C. Lim, R. Raj, . Acta Metall., (1984a) 32-1177.

[12] H. Mughrabi, R. Wang. Elsevier, 1988, pp.1.

[13] C. Blochwitz, J. Brechbühl , W. WTirschler, Analysis of activated slip systems in fatigued nickel polycrystals using the EBSD-technique in the scanning electron microscope. Mat. Sci. Eng., A 210 (1996) 42-47.

[14] J. Man, K. Obrtlik, C. Blochwitz, J. Polak, Atomic force microscopy of surface relief in individual grains of fatigued 316L austenitic stainless steel. Acta Mat., 50 (2002) 3767-3780.

[15] C. Perrin, S. Berbenni, H. Vehoff , M. Berveiller M, . Acta Mater., (2010) 58-4649.

[16] C. Wejdemann, O. B. Pedersen, . Mat. Sci. Eng. , A (2004) 387-556.
[17] P. Evrard, M. Sauzay. J. Nucl. Mat, 405 (2010) 83-94.
[18] P. Neumann. Scripta Met. Mater., (1992) 26-1535.

[19] Y. Chuang , H. Margolin. Metall. Trans., (1973) 4-1905.
[20] H. Margolin , M. S. Stanescu. Acta Met., (1975) 23-1411.

[21] O. Diard, S. Leclercq, G. Rousselier, G. Cailletaud. Int. J. Plast., 21 (2005) 691-722.
[22] A. N. Stroh. Adv. Phys., (1957) 6-418.

[23] E. Smith, J. T. Barnby. Metal Sci. J., (1967) 1-56.
[24] D. Leguillon. Eur. J. Mech, A/Solids (2002) 21- 61
[25] D. Taylor, P. Cornetti, N. Pugno . Eng. Fract. Mech., (2005) 72-1021.

[26] Cottrell, A.H., Theory of brittle fracture in steel and similar metals, 1958, Transactions of the metallurgical society of AIME, Vol. 212, p. 192-203.
[27] M. Sauzay, K. Bavard, W. Karlsen, TEM observations and finite element modeling of channel deformation in pre-irradiated austenitic stainless steels – interactions with free surfaces and grain boundaries. J. Nucl. Mater., 406 (2010) 152-65.

[28] T. Tabata, H. Fujita, M. A. Hiraoka, K. Onish. Phil. Mag., A (1983) 47-841.

[29] Leguillon D., Sanchez-Palencia E (1987). Computation of singular solutions in elliptic problems and elasticity. John Wiley & Sons / Masson.

[30] http://www.matweb.com/